Charge transfer efficiency (CTE) in the WFC3/UVIS CCDs

S. Baggett, H. Bushouse, R. Gilliland, V. Khozurina-Platais, K. Noeske, L. Petro
Jan 7, 2011

1.0 Outline

These pages provide an overview of CTE in the WFC3/UVIS CCDs and the results of an on-orbit charge injection test, followed by a discussion of the options for mitigating charge transfer inefficiency (CTI)-induced effects in Cycle 19.

> Introduction
> CTE measured from external targets
> Charge injection test results
> Options for CTI mitigation
> Appendix – CTE measured from the internal stimulus

2.0 Introduction

Charge transfer efficiency (CTE) is a measure of how effectively the CCD moves charge from one pixel to another during the chip readout; a perfect device transferring all of the charge without any losses would have a CTE of 100%. In practice, defects in the silicon matrix trap charge and release it at a later time, on scales of microseconds to seconds. The traps can be intrinsic to the device, i.e., introduced during the manufacturing process, or develop over time as the result of radiation damage. Devices in low-earth orbit are particularly susceptible to accumulating damage, in large part due to regular passes through the South Atlantic Anomaly, where the Earth's Van Allen belts come closest to the Earth and generate regions of higher radiation rates.

The resulting CTI from such radiation damage causes a loss in source flux due to the traps as well as a systematic shift in the object centroid as the trapped charge is slowly released during readout in the direction away from the amplifiers. The flux losses at any given time are typically a function of 1) row number and sometimes column number, i.e. sources further from the amplifiers require more transfers to read out and thus encounter more traps, 2) source brightness, i.e., fainter sources lose proportionally more charge than brighter sources, and 3) image background, i.e., a higher background can fill some of the charge traps, thereby minimizing flux losses in the source signal.

As with other HST CCDs like WFPC2, STIS, and ACS, the new WFC3 camera is experiencing a degradation in CTE over time as well, an effect being monitored via external and internal data. The rate of increase of CTI in WFC3 is a few times greater than expected and will significantly affect faint source photometry during Cycle 19.

3.0 CTE in external targets

To assess the photometric and astrometric effects of charge transfer inefficiency (CTI) on science data, periodic observations of a stellar cluster are acquired. For WFC3, the external CTE monitor has imaged the rich open cluster NGC6791 in F606W and F502N, in Oct 2009, March 2010, and Sep 2010. Aperture photometry analysis was performed on short/long exposure image pairs, three pairs per epoch. In the absence of CTI, the total counts in the long and short exposures, scaled to exposure time, should be the same. With CTI, sources at a given position in the short exposures will exhibit more flux loss than sources in the same position in the longer exposures as a larger proportion of the smaller charge packet in the former is lost to traps. Furthermore, the flux loss depends on the source distance from the amp; the further from the amp, the more transfers are required to read out the charge thus exposing the charge packet to more traps and the more charge is lost. Sky background is also a factor: higher background can fill charge traps thereby minimizing flux losses in the source signal.

The CTI has been measured by computing ratios of the long to short exposure fluxes, obtained via aperture photometry (radius=5 pixels) and normalized by exposure times, and examining the behavior as a function of row (Y) position in the chip, total brightness of the target, and sky background level. In the absence of CTI-induced losses, these ratios should be unity; in the presence of CTI, there will be dependencies on row (and possibly column) position, source brightness, and sky background. The CTE loss reported in Table 1 is for moderately-bright stars (500-2000 e- total flux in the short exposure) and has been computed as the difference between the mean short/long flux ratio in the 500 rows closest to the amplifier and the mean short/long flux ratio in the 500 rows furthest from the amplifier.

In the F502N images, which have a background of only 0.1-1e-, moderately bright stars (500-2000 e- total flux in the short exposure) showed a CTE loss of ~2.5% about five months after installation, 4.5% flux loss just under a year after installation and 7% about 16 months after installation. Measurements using a different star cluster, discussed in more detail in the Charge Injection section, yielded ~8% loss at ~17 months after installation. The F606W images, with higher background (1-30e-), showed an average CTE loss of ~2.5% after 16 months in operation (Khozurina-Platais et al., 2011). Note that these values are lower limits due to the analysis technique of comparing differential CTE losses between long and short exposures as well as binning stars in the 500 rows closest to, and in the 500 rows furthest from, the amplifiers. That is, the CTI losses are across an average parallel shift distance of 1550 rows and those are losses in the short exposures using a long exposure for reference. Since the long exposures will have incurred some small loss as well, the tabulated values are likely underestimates at the ~25% level.

Table 1. Average CTE losses in percent as a function of time for the WFC3 CCDs, based on aperture photometry of moderately bright stars (defined as 500-2000 e- in the short exposure).

Date	Days since launch	F502N		F606W		Target
		CTI(%)	error	CTI(%)	error	
Oct 2, 2009	144	2.4	0.4	1.1	0.4	NGC 6791
Mar 25, 2010	318	4.5	0.4	1. 0	0.4	NGC 6791
Sep 2, 2010	479	6.8	0.4	2.6	0.4	NGC 6791
Sep 27, 2010	504	8.2	0.5	N/A		NGC 104 (47 Tuc)

Furthermore, the CTE losses measured for these moderately bright targets (500-2000 e- total flux in the short exposure) appear to be a factor of 2-3 greater than what would have been expected based on the ACS performance in its first years on-orbit in 2002/2003 (Chiaberge et al., 2009). However, the faster degradation seen in 2009/2010 also appears to be occurring on ACS as well (Massey, 2010; Ferguson, B., priv.comm.). One possible contributing factor is the solar minimum: 1) the strength and extent of the SAA, where most of the CTI-inducing traps are thought to be formed, is known to be anti-correlated with solar activity (e.g., Casadio et al. 2010) and 2) the installation of WFC3 on HST coincided with solar minimum while the installation of ACS occurred during a period of higher solar activity. As shown in Figure 2, using the Casadio SAA area index and flux index data from the ATSR instruments (Along Track Scanning Radiometer) on-board the ESA ERS and ENVISAT satellites as a proxy for estimating radiation exposure, the exposure levels at the time of WFC3 installation in 2009 were significantly greater than those in 2002 when ACS was installed, in rough agreement with the CTE measurements. The figure presents the SAA area index (red), flux index (blue), and resulting SAA exposure index (flux*sqrt(area); green curve) trends as a function of time. The operational dates of the HST CCD detectors are indicated via the horizontal bars along the top of the figure, with the four epochs of data used for the ACS CTE measurements (Chiaberge et al., 2009) superposed as circles. The tri-color Wide Field Camera bar marks the epochs of the cameras which have occupied HST's radial bay over the course of the mission: WF/PC1 (1990-1993), WFPC2 (1993-2009), and WFC3 (2009+).
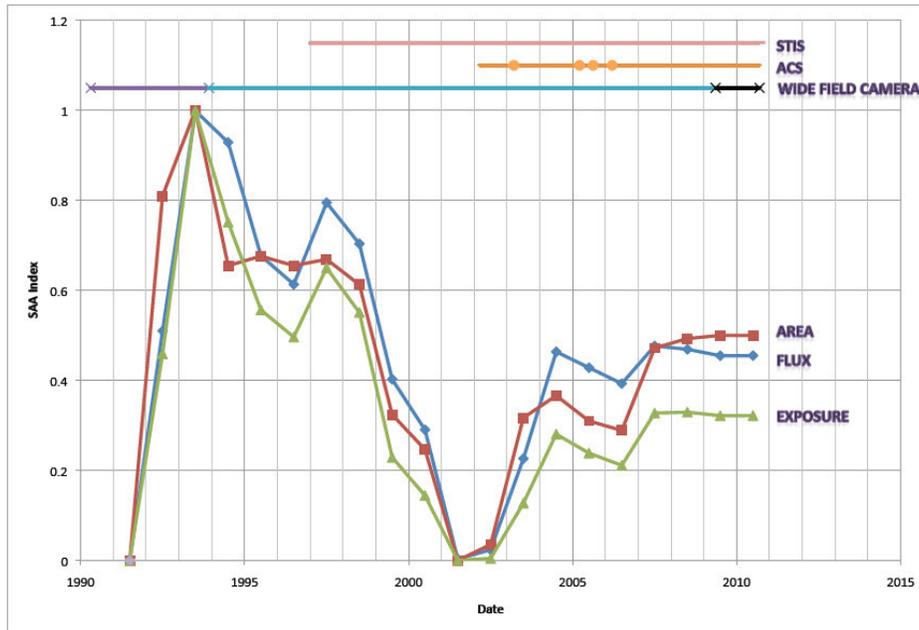
Fig. 2 HST exposure to on-orbit radiation as a function of year. Results are based on SAA area index and flux index from the ATSR spacecraft. Minimum exposure occurred ~2002/2003 (early years of ACS); exposure levels in 2009/2010 (first years of WFC3) are significantly greater.

Regardless of the cause, if the CTE degradation continues at this rate, moderately bright sources (500-2000 e- total flux) in low sky background images will experience >16% losses in May 2012 (Cycle 19 observations nominally run from Oct 2011 through Sep 2012) while very faint sources may suffer losses of several 10's of percent. With such significant flux losses, observers will need to consider how best to mitigate the effect for their project.

4.0 Charge injection test results

As an option for mitigating CTE degradation, WFC3 has the capability of electronically inserting charge into the CCD with a lower noise penalty than the traditional pre or post-flash techniques. The injection is performed by reversing the voltage in the charge dump gate which allows the charge to flow into the detector; appropriate timing controls the number of rows receiving charge. In WFC3, the CCDs are able to inject charge every 10th, every 17th, every 25th, or every row (continuous). The level of charge is ~17000 electrons, is highly repeatable (+/- ~0.5e-), and serves effectively as a preflash but with considerably lower noise, ~15-20e- in the CI rows. The CI mode is expected to be offered as an option to observers in Cycle 19, accessible via an Optional Parameter in the Phase II APT software.

An on-orbit test of the WFC3 charge injection capability has been executed to evaluate the performance of the different modes (proposal 12348). The program was structured as five visits, one orbit per visit,

with one CI mode tested per orbit, plus a control (no CI). The target was the globular cluster NGC104 (47Tuc), also used for ACS CTE monitoring. Filter F502N was chosen so as to minimize the sky background, thereby maximizing any CTI effects. The orbit visibility was such that 8 images could be taken: these were divided into two short and two long exposures at two pointings offset by about 1 chip height, or half the total WFC3 FOV. Each long and short pair was also dithered by a small amount (2.5 pix in X and Y) to allow for cosmic ray and hot pixel rejection. A set of internal biases and darks were also obtained, about 20 in each mode, in order to allow construction of a CI-mode specific superbias. Fig 3 shows one subsection of an image taken with charge injection every 10th row; at left is the injected image after subtraction of a normal (no CI) superbias while at right is the same external CI image with a CI-superbias removed. As can be seen in the figure, some noise remains in the CI lines (~15-20e-); in addition, the level of noise in the regions away from the CI rows is slightly higher (4-5 e-, depending on distance from the amps and CI rows) than that in an image without CI. The level of noise in the rows away from the CI is never quite as low as in an image without CI (Fig 4). In addition, a slight residual signal (few e-) remains in the CI rows of a CI-superbias subtracted frame; observers planning to use CI should assume that the CI rows may need to be discarded during processing, e.g., assigned zero weight when combining multiple, dithered exposures.
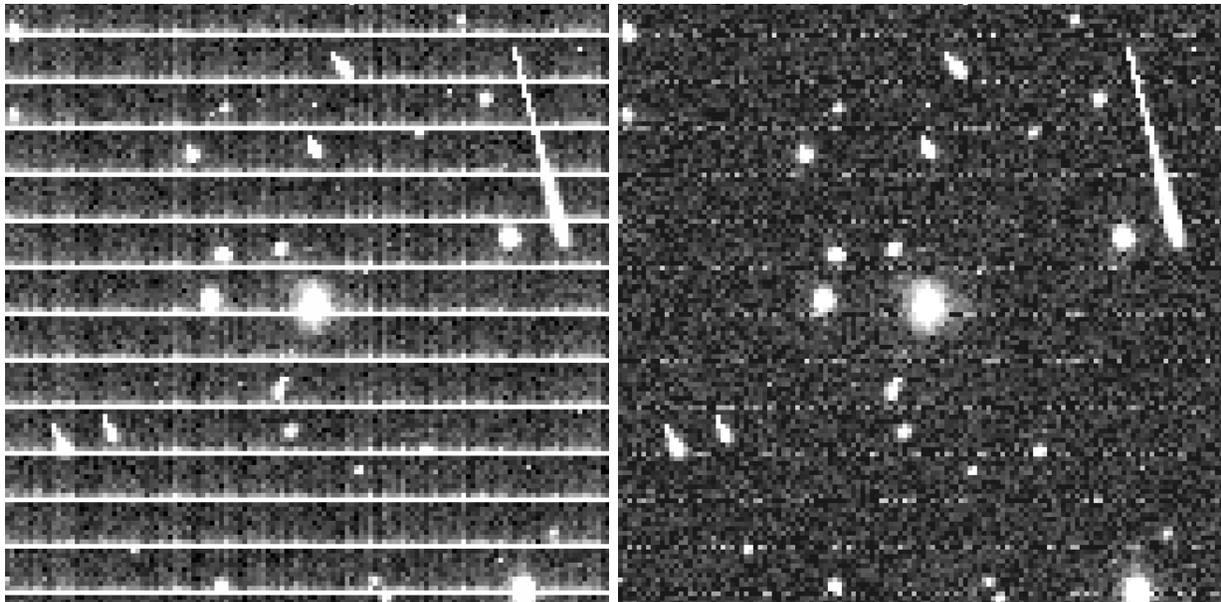

Fig. 3 At left, a section of a charge-injected image with normal bias subtraction; at right, the CI image after application of a CI superbias.
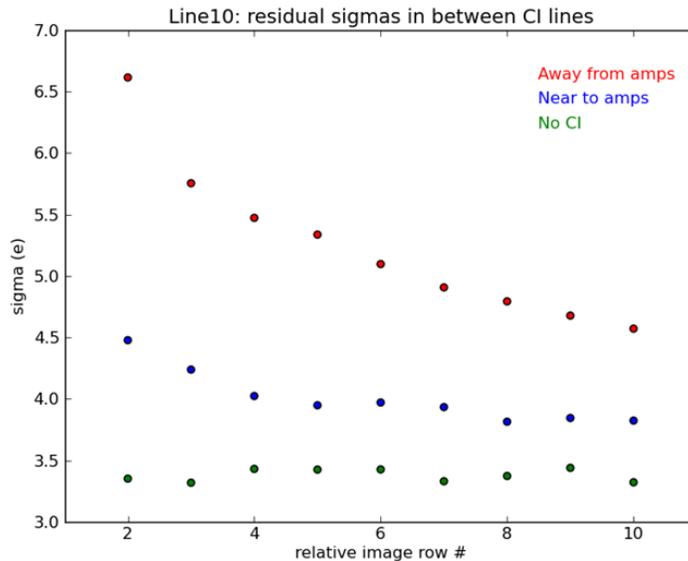
Fig.4 Residual noise in the 9 non-CI rows of an external image with CI injected every 10th row, after an appropriate CI superbias subtraction; the upper curve of points (red) are from rows far from the amplifiers while the middle curve of points (blue) are from rows close to the amplifiers. For comparison, the green values (lowest set of points) show the residual noise in those same rows for the non-CI injected image.

For the CI evaluation, standard aperture photometry was performed on the calibrated (flt) images using a radius of 3 pixels. For moderately bright stars (total flux of 500-2000e- in the short exposure), ratios of the long to short exposure count rates were plotted as a function of row (Y) position in the WFC3 FOV. Due to the positions of the amplifiers (Y=0 for UVIS2, Y=4096 for UVIS1), the CTI-induced photometric losses generate the inverted V-shape seen in Fig 5. The CTE loss is expressed as a loss in flux for the short exposure relative to the long exposure between the stars in the 500 rows closest to the amplifiers and in the 500 rows furthest from the amplifiers. A comparison of photometric results from the CI images to the control (no CI) image has shown that the 10th-row injection mode was able to provide the most effective CTE recovery though the other two line modes were able to provide a significant improvement in CTE (Bushouse et al., 2011).

A complementary analysis of the same data set, using calibrated, drizzled products (drz) and comparing aperture photometry fluxes in the pair of long exposures at one pointing to those in the pair of long exposures at the second pointing has also shown that the discrete CI line modes provide significant improvement in the measured fluxes compared to the non-CI image.
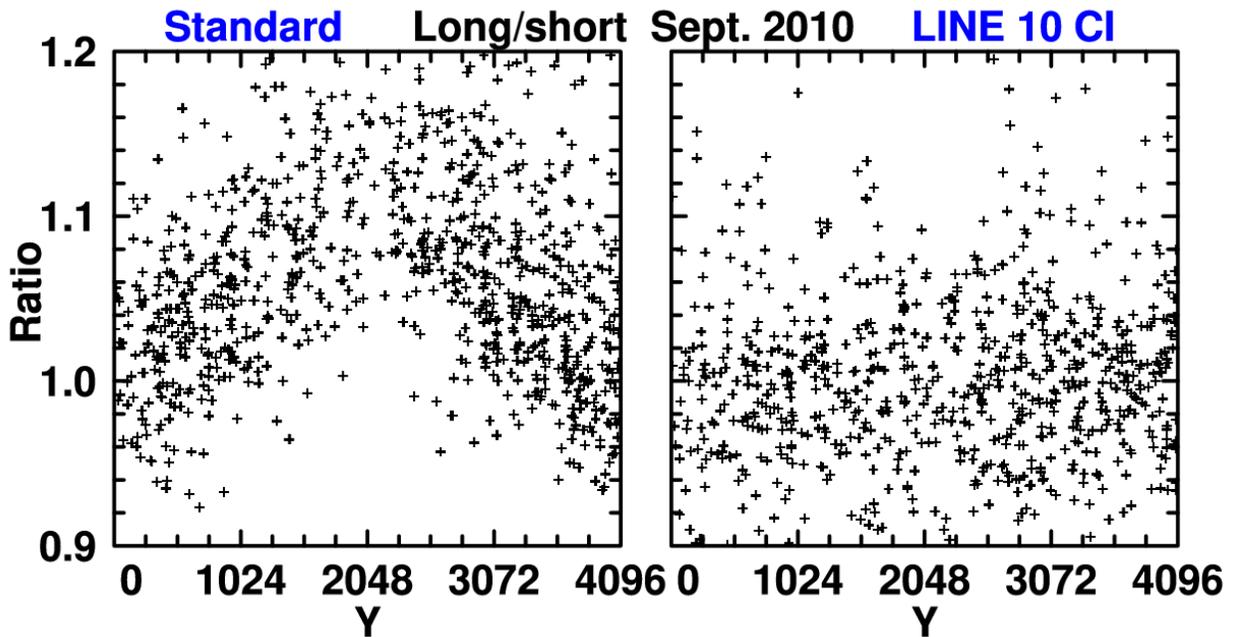
Fig.5 Ratio of 47 Tuc aperture photometry fluxes in the long exposure compared to the short exposure, taken at the same pointing (for stars with 500-2000e- total in the short exposure). At left is the result for the non-CI image while at right is the result for the line 10 CI image.

5.0 Options for mitigating CTI-induced effects

As presented in the previous sections, the WFC3 CCDs are showing signs of CTI as expected; however, along with ACS, the CTE degradation in 2009/2010 appears to be occurring faster than in earlier years, likely a consequence of the solar minimum which increases radiation levels in South Atlantic Anomaly (SAA). For example, for moderately bright sources in a low background (500-2000e- total flux and 0.1-1e-, respectively), the CTI in WFC3 was at the ~2.5% level in the fall of 2009 and at the ~7% level in the fall of 2010; if the trend continues, the flux losses will be >16% in March 2012. Extrapolation into 2012 of losses for bright sources and/or images with high background is more uncertain but estimated at ~5%. Observers in Cycle 19 and beyond will want to consider options for reducing the effects.

In some science cases, options to mitigate CTI effects may include placement of the target near the amplifiers to minimize the number of transfers during readout (feasible only for small targets) or use of a broader filter and/or longer exposure time in order to simultaneously increase the sky background and signal level. Observers may also consider the application of a correction after the data are in hand, via e.g. photometric formulae (Chiaberge et al., 2009) or a pixel-based correction (Anderson & Bedin, 2010) as done for ACS, or application of charge injection before the data are taken. Each of these options entails advantages and disadvantages.

5.1 CTI correction after data acquisition

The greatest benefit of a correction applied during data processing is that the procedure happens after the data are acquired. Thus, if changes to the correction are made at some later time, either algorithm enhancements or bug fixes, the data can be reprocessed to take advantage of the improvements. There is, however, a chance that the algorithm may never be able to completely recover what was lost. Faint sources, and faint features of extended sources, may be so strongly affected by CTE that they become undetectable and cannot be recovered. Also, faint information that is still detectable will be affected: processing low signal to noise data by, e.g., a deconvolution algorithm can yield uncertain results, generally amplifying noise or, sometimes, generating artifacts. Finally, there are currently no aperture photometry CTI corrections available for WFC3. In addition, while the development of an empirical pixel-based correction algorithm has been successful for ACS data, no such correction exists yet for WFC3 data. Work on a pixel-based correction for WFC3 is planned to begin Spring 2011; the expectation is that a preliminary implementation of a standalone task, along with an assessment of its efficacy, will be available for observers before the Cycle19 Phase II due date, i.e., before the decision must be made as to whether CI should be used.

5.2 CTI correction before data acquisition

5.2.1 Advantages and Disadvantages of CI

The benefit of CI is that it has been shown in ground and on-orbit tests to be effective at significantly reducing the flux lost to CTI. No extra calibration processing is intended to be required on the part of the observer, the CI is performed on the instrument before the data are acquired and the calibration pipeline applies the appropriate CI reference file. However, a disadvantage is that the CI process is permanent: once charge is injected, it can not be undone. Furthermore, CI generates a small amount of additional noise in the image, for a total of 4-5e- rms in non-CI rows, as opposed to ~3.5e- total noise in equivalent non-CI images*;* **observers considering use of the CI mode should note that the Exposure Time Calculator does not take the extra noise into account.** The small amount of additional noise should have relatively little effect on bright targets and/or images with relatively high sky background but will of course have a more significant effect on fainter targets and/or images with low sky background (e.g., those taken with narrowband or UV filters). Finally, when computing the number of required orbits, observers planning to use the CI mode in Cycle 19 should assume that the CI rows (every 10th row) will likely be unusable, requiring the use of dithered sets of exposures.

5.2.2 Effects of CI on UVIS data and adjusting the integration time

   As discussed above, charge injection adds some additional noise and requires proper dithering to remove the charge-injected rows. Observers may have to adjust their integration times accordingly. We assume here that every 10th row will be charge-injected, which would require the biggest adjustments.

1) To remove the charge-injected line, exposures should be broken up into several dithered ones; as this is something that the majority of programs are already doing, no additional overhead is incurred. However, since every 10th row may have to be discarded, total time requirements may increase by 10%.

2) The increased noise due to CI will not strongly affect observations with high backgrounds, e.g., long exposures in filters such as F606W and F814W, though the noise may be an issue for observations with low backgrounds. The WFC3 ETC (http://etc.stsci.edu/etc/input/wfc3uvis/imaging/) can provide estimates of the sky levels for specific observing scenarios but typically broadband and some medium band filters in the visible and red will be skynoise-dominated while the UV and narrow-band filters will be read(CI)noise-dominated. For example, in a 1000 sec exposure with default levels of zodiacal light and earthshine, F606W, F547M, F657N, F275W, and F656N will have sky levels of ~55, ~25, 3, 0.8, and 0.4 e-/pixel, respectively.

While the ETC does include the readnoise (nominally ~3 e-/pixel), it does not take additional noise sources, like CI, into account; observers can estimate how their data may be affected by CI by obtaining approximate noise levels from Fig. 4. Without CI, the background noise in these essentially zero-background data is about 3.4 e-, almost the UVIS read noise level. The worst affected data are rows adjacent to the CI rows, far from the amplifier, where the noise may be twice that level (6.5 e-). This does moderately affect high-background applications (e.g. broad band imaging in the visual). For the worst cases such as observations of faint sources in very low backgrounds, the additional noise can be a concern if the source cannot be placed close to the amplifier or away from CI rows such as for a sky survey.

For example, consider very low background dithered observations in F656N, 1000 sec, V=21, with CI and an average noise of ~5e-. An extra ~30% observing time will be required to reach the same S/N level as without CI; a V=25 target in the same scenario will require ~50% extra time. However, these should be the worst cases; more typical observing scenarios, e.g. F606W with CI, would require ~10% additional observing time to achieve the same S/N level as an image without the additional CI noise. Alternately, the loss of sensitivity can be considered; for example, for S/N=5, observing with CI will result in a loss in limiting magnitude of ~0.1 mag in F606W and 0.4-0.5 mag in F275W, F657N, and F656N. These examples, along with a few others, are summarized in Table 2 below. For each observation (target type, brightness, filter), the target, sky, and dark levels achieved in 1000 sec are listed, in electrons as measured in a 5x5 pixel box, along with the predicted S/N assuming no CI (ETC) and S/N assuming CI (readnoise+CI noise of 5e-). The next to last column provides an estimate of the exposure time factor required to achieve the same S/N as in the 1000 sec exposure, including allowances for the additional sky and dark accumulated during that extra exposure time. The last column shows the loss of limiting magnitude in 1000 sec exposures, taking the magnitude of a S/N = 5 target as the limiting magnitude.

Proposers will want to carefully weigh the advantages and disadvantages of CI, or other CTE mitigation methods, in achieving the required science goals. Questions and concerns may be directed to the STScI helpdesk (help@stsci.edu).

Table 2. Sample S/N calculations for the given observing scenario; target, sky, and dark levels are the total number of electrons in a 5x5 pixel box. Two S/N values are listed: the first is computed using the ETC assumptions (no CI) and the second assuming read+CI noise of 5e-. The next to last column indicates the exposure time factor required to achieve the same S/N as a 1000-sec non-CI observation and the last column gives the loss of limiting magnitude of a 1000-sec CI exposure as compared to a non-CI exposure (for a S/N=5 target).

Scenario	Exptime (sec)	Target	Sky	Dark	S/N (ETC)	S/N (5e-)	Exptime factor (CI)	Loss of lim mag (S/N=5)
K0III, 5x5 box, V=25,F606W	1000	2375	1378.3	12.5	37.6	35.8	1.09	0.11
B0III, 5x5 box, V=25,F606W	1000	1921	1378.3	12.5	32.3	30.6	1.10	0.11
Flatspec(ν) , 5x5 box, V=25,F606W	1000	2100	1378.3	12.5	34.4	32.7	1.09	0.11
Flatspec(ν), 5x5 box, V=28,F606W	1000	152.5	1378.3	12.5	3.6	3.27	1.18	0.11
Flatspec(ν), 5x5 box, V=30,F606W	1000	24.2	1378.3	12.5	0.6	0.54	1.19	0.11
K0III, 5x5 box, V=25, F657N	1000	125	70.3	12.5	6.0	4.3	1.47	0.45
Flatspec(ν), 5x5 box, V=22, F657N	1000	2048	70.3	12.5	42.2	39.0	1.14	0.45
Flatspec(ν), 5x5 box, V=25, F657N	1000	90	70.3	12.5	4.5	3.2	1.49	0.45
K0III, 5x5 box, V=25,F275W	1000	2.3	19.6	12.5	0.1	0.09	1.57	0.40
B0III, 5x5 box, V=25,F275W	1000	636.3	19.6	12.5	21.3	17.7	1.29	0.40
Flatspec(ν), 5x5box, V=21, F275W	1000	3309	19.6	12.5	55.4	52.5	1.10	0.40
Flatspec(ν), 5x5box, V=21.5, F275W	1000	2088	19.6	12.5	43.1	39.8	1.14	0.40
Flatspec(ν), 5x5box, V=26, F275W	1000	33.1	19.6	12.5	1.9	1.3	1.58	0.40
K0III, 5x5 box, V=21, F656N	1000	681	9.2	12.5	22.4	18.7	1.28	0.46
Flatspec(ν), 5x5box, V=16, F656N	1000	70902	9.2	12.5	265.8	265.1	1.01	0.46
Flatspec(ν), 5x5box, V=21, F656N	1000	709	9.2	12.5	22.9	19.3	1.28	0.46
Flatspec(ν), 5x5box, V=26, F656N	1000	7.1	9.2	12.5	0.4	0.3	1.65	0.46

6.0 References

Anderson,J., and Bedin, L., "An Empirical Pixel-Based Correction for Imperfect CTE. I. HST's Advanced Camera for Surveys," PASP, 122:1035-1064, 2010.

Bushouse, H., Baggett, S., Gilliland, R., Petro, L., "UVIS Charge Injection Test", WFC3 ISR 2011-02.

Casadio, S., Arino, O., and Serpe, D., "Monitoring the South Atlantic Anomaly using ATSR," presented at ESA Living Planet Symposium; Bergen, Norway; June 28 – July 2, 2010).
http://due.esrin.esa.int/wfa/LPS_SAA_1869182_Casadio.pdf

Chiaberge, M., Lim, P-L., Kozhurina-Platais, V., Sirianni, M., and Mack, J., "Updated CTE photometric correction for [ACS] WFC and HRC,", ACS ISR 2009-01.

Janesick, J.R., "Scientific Charge-Coupled Devices", SPI Press, Bellingham, VA, 2001.

Kozhurina-Platais, V., Baggett, S., Hilbert, B., Gilliland, R. "Internal Monitoring of the WFC3/UVIS Charge Transfer Efficiency," HST Calibration Workshop 2010,
http://www.stsci.edu/institute/conference/cal10/posterList

Khozurina-Platais, V., Hilbert, B., Martel, A., McCullough, P., "WFC3/UVIS CTE-EPER Measurement,", WFC3 Instrument Science Report 2009-10.

Khozurina-Platais, V., Gilliland, R., and Baggett, S., "WFC3/UVIS-Cycle 17: CTE External Monitoring – NGC6791,", Jan 2011 (in preparation).

Massey, R., "Charge Transfer Inefficiency in the Hubble Space Telescope since Servicing Mission 4," MNRAS in press. (http://arxiv.org/abs/1009.4335)

Robberto, M., " UVIS CCD EPER CTE measurements performed during the April 2007 Ambient Calibration campaign (SMS UV02S01)," WFC3 Instrument Science Report 2007-13.

7.0 Appendix

CTE based on internal data

For completeness, we include here a brief summary of CTE monitoring based on internal observations. Note, however, that while the CTI behavior measured via EPER data is useful for monitoring purposes in a relative sense, external observations taken in the same mode as external science images are necessary to quantify the CTI effects on photometry and astrometry.

Charge transfer inefficiency (CTI)-induced losses are monitored via internal exposures taken roughly every month using the EPER (Extended Pixel Edge Response) method. EPER data consist of internal tungsten lamp flat field exposures which are read out in a special format resulting in less imaging area pixels but significantly more area of overscan. The EPER flat fields are taken with various filter/exposure time combinations to provide a range of illumination levels (from ~150 e- to 5000 e-). By measuring the signal profiles as they extend into the trailing overscan region, an assessment can be made of the relative CTE level. Specifically, the EPER CTE is computed as

$$CTE(eper) = 1.0 - S(D) / [N \times S(LC)]$$

where S(D) is the total amount of deferred charge in electrons within the overscan region, S(LC) is the charge, in electrons, in the last column of trailing overscan, and N is the number of transfers required to read out (Janesick, 2001).

The decline in CTE since launch as a function of time (Modified Julian Date) and source brightness (legend at left) based on the EPER data is shown in Figure 6. As expected, the rate of decline is significantly less for high signals than low signals. Analysis details are available in Khozurina-Platais et al. 2010, Khozurina-Platais et al. 2009, and Robberto 2007.
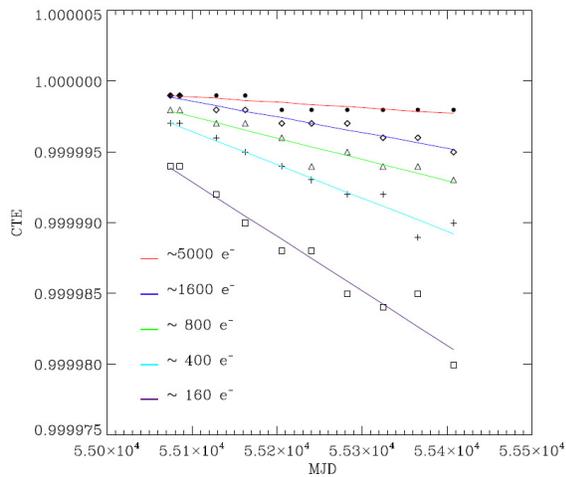

Fig.6 EPER CTE as a function of time and source brightness.